Ionization energies of amphoteric-doped Cu_2ZnSnS_4: Photovoltaic application

C. Tablero

A B S T R A C T

The substitution of Cu, Sn or Zn in the quaternary Cu_2ZnSnS_4 semiconductor by impurities that introduce intermediate states in the energy bandgap could have important implications either for photovoltaic or spintronic applications. This allows more generation–recombination channels than for the host semiconductor. We explore and discuss this possibility by obtaining the ionization energies from total energy first-principles calculations. The three substitutions of Cu, Sn and Zn by impurities are analyzed. From these results we have found that several impurities have an amphoteric behavior with the donor and acceptor energies in the energy bandgap. In order to analyze the role of the ionization energies in both the radiative and non-radiative processes, the host energy bandgap and the acceptor and the donor energies have been obtained as a function of the inward and outward impurity-S displacements. We carried out the analysis for both the natural and synthetic CZTS. The results show that the ionization energies are similar, whereas the energy band gaps are different.

1. Introduction

The quaternary Cu_2ZnSnS_4 (CZTS) semiconductor has a variety of interesting physical properties and with a wide range of potential applications in device technology. Among these properties, the bandgap energy (1.4–1.6 eV) and high absorption coefficient ($\alpha \sim 10^4\,cm^{-1}$) stand out. In addition CZTS have relatively abundant constituents, at a low-cost, and are non-toxic.

CZTS has been experimentally obtained and prepared by several methods: the sulfurization of sputtered [1–3] or evaporated [4] stacked films, spray method [5,6], sol–gel method [7], hydrazine deposition [8], and electrode deposition [9]. Their properties have been extensively studied both experimentally [10–18] and theoretically [19–26]. The experimental samples mainly crystallize in the kesterite structure, although a stannite-type structure can be formed through a two step process [27].

Although the kesterite- and the stannite-type structures do show any differences, it is rather difficult to distinguish one from the other experimentally as these structures have similar cell volumes and internal atomic positions. In addition, both structures are nearly degenerated energetically [21–23]. Therefore, it is likely that the two structures coexist in experimental samples [14,15] leading to phase mixing.

Even in undoped CZTS the cation substructure turns out to be intrinsically disordered. The exchange between Cu and Zn only results in a minimal energy penalty and causes a significant lowering in symmetry [21–23]. The Cu/Zn disorder is difficult to measure experimentally since the atomic scattering form factors are proportional to the atomic number, and the Cu and Zn positions are not easy to differentiate. Therefore, although the CZTS structure without cation disorder has been predicted to be the most stable [21,22], possible a Cu/Zn cation disorder in experimental samples cannot be excluded [21–23].

Intrinsic disorder in CZTS, i.e. the presence of vacancies, antisite atoms, etc., are what gives rise to the doping behavior [21–24]. The observed *p*-type conductivity comes mainly from the intrinsic Cu_{Zn} antisite with a relatively deeper acceptor level. In addition, the inter-mixing of host atoms with different oxidation states, such as the Sn/Zn cation disorder [24] can gives rise to deeper levels in the energy band gap.

Therefore, systematic control of intrinsic defects in growing and non-equilibrium growth techniques may be required to avoid the formation of secondary phases by using kinetic energy barriers [20]. This would improve the crystallinity and the solar cell performance.

Because of the large variety of isolated intrinsic point defects and structures, the experimental and theoretical studies are currently focusing on the impact of structural modifications. However, there are few studies on the isolated substitutional impurities.

The insertion of intermediate states into the energy bandgap of a host semiconductor can modify the optoelectronic properties of the host. In particular, it could provide additional paths for optical transitions making these compounds interesting for optoelectronic

applications. For example, solar-cell devices based on a material with three defined absorption bands in a simplified one-junction structure can increase the efficiency as regards single-gap solar cells [28]. The absorption of photons is more efficient than in conventional single-gap cells because the absorption of low energy photons causes transitions from the valence band (VB) to the partially filled intermediate band (IB) and from there to the conduction band (CB). These transitions generate additional carriers to those generated for the usual process through photon absorption, promoting electrons from the VB to the CB.

Some host semiconductors and impurities have been analyzed in order to insert intermediate states into the energy band gap: doped chalcopyrites [29–32], II–VI compound doped with isoelectronic oxygen impurities, Cr-doped zinc chalogenides [33,34], etc. In particular, the isoelectronic doping with oxygen of some II–VI semiconductors has shown that oxygen gives rise to deep traps [35–38] in which carriers recombine radiatively [39–43]. Cr-doped zinc chalogenides [44–46] have been used as broadly tunable continuous wave lasers with negligible non-radiative decay at room temperature. Cr-doped CZTS present several recombination paths depending on the IB occupation and on the cation substitution [26].

However, the influence of the impurities on the lattice dynamic has not attracted as much attention, despite its importance in radiative and non-radiative processes. For example, in the interaction of impurity electrons with light, the Coulomb field of the charged impurity center displaces the nearest neighboring atoms via a breathing mode, which may affect its properties. When the impurity acceptor energy crosses the CB because of the breathing mode, an electron in the CB can be captured non-radiatively by the impurity (Fig. 1). Similarly, when the impurity acceptor energy crosses the VB, an electron in the impurity can be captured non-radiatively by the VB. In this way it closes the cycle of non-radiative recombination from an electron in the CB to an electron in the VB [47,48].

In addition, the energetic positions of the donor (e_D) and acceptor (e_A) ionization energies allow an easy characterization of the impurity as a donor (e_D lies in the gap but e_A does not) an acceptor (e_A lies in the gap but e_D does not) or with amphoteric behavior (both e_D and e_A i.e., the lower and upper Hubbard bands, are found within the gap). This behavior can be very important for the radiative and non-radiative transitions [49,50], as well as in the application of these compounds for optoelectronic devices. It could have a negative effect because these deep localized defect states at low concentration act as effective non-radiative recombination centers as previously mentioned. However, at high concentration the defect states lead to bands. If the bands corresponding to the ionization energies overlap, there is the possibility of forming a partially filled IB. For a partially filled IB the donor and acceptor energies coincide with the Fermi energy, i.e. the IB has amphoteric behavior. On the other hand, the limits of the IB for a larger impurity concentration would lead to two energy levels for lower impurity concentration via a metal–insulator transition. In order to form a band, the impurity concentration should exceed the threshold set by the Mott's transition ($\sim 10^{19}$ cm^{-3} [49]). Then, the modification of the charge density around the impurity as consequence of the electronic capture of the non-radiative mechanism is redistributed among all the impurities [49] or with the host semiconductor [50], and the negative non-radiative recombination would be decreased. Experimental evidence supporting this theory was reported by measuring the lifetime of titanium implanted silicon wafers [51].

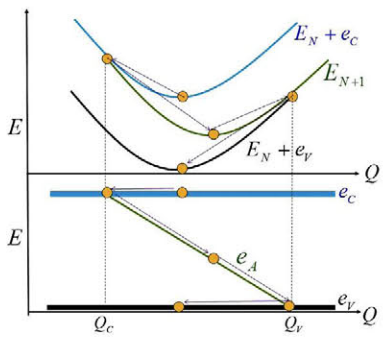

Fig. 1. Schematic representation of the non-radiative recombination with respect to the configuration coordinate Q. Q_C (Q_V) is the crossing point of the ionization e_A and CB (VB) edge e_C (e_V) energies.

The technological importance of CZTS as an absorbent material for low-cost thin-film solar cells together to the possible additional improvement in their optoelectronic properties for inserting states into the energy band gap leads us to explore the effect of the substitution of first row transition-metal atoms at cation substitutional CZTS sites. After a general screening, V, Cr and Ir have been identified as interesting impurity candidates, i.e. with amphoteric behavior at the nuclear equilibrium configuration, to obtain intermediate states within the main gap of the modified CZTS. In order to analyze the effect on the non-radiative processes (Fig. 1), the ionization energies have been obtained at the nuclear equilibrium configurations corresponding to a breathing mode.

The results in this work refer to ideal stoichiometric CZTS lattice structures, in the sense that no intrinsic point defects nor combinations of them other than the specific substitution proposed have been allowed. It is assumed that the substitutional impurities have no interaction with other intrinsic point defects. Hence, the substitutional impurity results also add to the results of isolated point defects and complexes. It is expected that these results may guide future experimental work in CZTS compounds for optoelectronic applications. Even if some impurities do not have attractive optoelectronic properties, they could have potential applications in spintronic devices. To achieve this objective, firstly, the position in energy of the donor and the acceptor ionization levels will be determined for both the natural and synthetic CZTS, comparing the results with the literature. Secondly, the evolution of the ionization levels with respect to the M–S distance will be obtained. From these results, the relative influence of radiative and non-radiative processes will be analyzed.

2. Calculations

Defect levels are usually characterized using a single-particle picture. But these single-particle eigenvalues do not account for the excitation aspect inherent in the ionization or recharging of the defect. Therefore, in order to obtain the donor (e_D) and acceptor (e_A) ionization energies we used total-energy differences [52,53] instead of single-particle energies.

The formation energy needed to incorporate one positive (negatively) charged M atom into place B (M_B substitution) in the host H semiconductor, and thus form a donor (acceptor), is $\Delta H_f(M_B^{\pm}) = E(M_B^{\pm}) - E_H + \mu_B - \mu_M \pm E_F$, where $E(M_B^{\pm})$ denotes the total incorporation energy, E_H is the total energy of the host, E_F is the Fermi energy, and μ_B and μ_M denote the chemical potentials of the B and M. These chemical potentials represent the energy of the reservoirs with which atoms are being exchanged. Therefore the incorporation will be favored if more M atoms are available (higher μ_M), if more B places are available (lower μ_B), and if the position of E_F is lower (higher). The ionization energies correspond to the value of E_F at which the impurity or defect changes from $M_B^{\pm}$ to M_B, i.e. $e_A = E(M_B^-) - E(M_B)$ and $e_D = E(M_B) - E(M_B^+)$. For the host semiconductor, when B = M, the acceptor and donor energies correspond with the CB and VB edge energies, i.e. e_C and e_V, and the gap is $E_g = e_C - e_V = E(M_M^-) - 2E_H + E(M_M^+)$.

In order to obtain the total energies needed to obtain the ionization levels, we use the density-functional theory. The standard Kohn–Sham [54] equations are solved self-consistently [55]. The standard Troullier–Martins [56] pseudopotential for the core orbitals is adopted and expressed in the Kleinman–Bylander [57] factorization. The valence wave functions are expanded in a localized pseudoatomic orbital basis set [58]. The pseudopotentials used to describe the exchange correlation energy were carried out with the generalized gradient approximation (GGA) from Perdew, Burke, and Ernzerhof [59]. All calculations were made with periodic boundary conditions and spin polarization.

The primitive cell of the kesterite-type structure (space group is $I\bar{4}$) is base-centered tetragonal with 8 atoms/cell. The experimental [60] lattice parameters of the natural CZTS (HLP) are: $a_H = 5.427$ Å and $c_H/2a_H = 1.002$. However, natural CZTS often contains Fe. An experimental analyses of the synthetic (iron-free) CZTS [61] reports different cell parameters (SLP) $a_S = 5.485$ Å and $c_S/2a_S = 0.997$. Because these experimental parameters are different, we are going to analyze both to compare their effect. In CZTS, the Cu can occupy the 2a and 2c crystallographic non-equivalent positions according to the Wyckoff labelling scheme. The electronic energy structure only has slight differences [26]. Therefore we have discussed only the 2a substitution.

In order to analyze the CZTS:M alloys ($(M_xCu_{2-x})ZnSnS_4$, $Cu_2(M_xZn_{1-x})SnS_4$ and $Cu_2Zn(M_xSn_{1-x})S_4$ for the M_{Cu}, M_{Zn}, and M_{Sn} substitutions respectively) we use 64-atom supercells ($x = 0.083$). In all of the results presented in this work, a double-zeta with polarization functions basis set has been used with periodic boundary conditions and 24 special k-points in the Brillouin zone. Larger supercells (from 144 to 216 atoms) have only been used in a few cases in order to compare them with 64 atom supercells.

3. Results and discussion

According to the ionic model, it is common to regard CZTS with the formal charges $Cu_2^+Zn^{2+}Sn^{4+}S_4^{2-}$. When the impurity M substitutes cation with a charge state $+p$ ($p = 1,2$ and 4 for the M_{Cu}, M_{Zn}, and M_{Sn} substitutions), donor-type ($M^{p+}/M^{(p+1)+}$) as well as acceptor type ($M^{p+}/M^{(p-1)+}$) conversions are conceivable. The energies associated with these transformations are the donor (e_D) and acceptor (e_A) ionization energies respectively. The energy range in which these oxidation states are stable depends on the Fermi energy. For example, the oxidation state M^{p+} is stable when the Fermi energy is between the acceptor e_A and the donor e_D ionization energies. When the Fermi energy is above e_A or below e_D, the $M^{(p-1)+}$ and $M^{(p+1)+}$ will more stable respectively. In general, the stability of positive oxidation states decreases as the Fermi energy shifts from the VB to the CB.

With the purpose of analyzing the possible amphoteric behavior (both e_D and e_A are found within the gap) the host gap and the donor and acceptor ionization energies have been obtained for all substitutions of host cations by M (M_A substitutions, with A = Cu, Sn and Zn, and M = V, Cr and Ir) in accordance with the calculations section. In order to analyze the possible effect on the non-radiative transitions, the dependence on the energy gap and the ionization energies with the impurity atomic environment have been obtained as a function of the inward and outward displacement of the nearest S neighbors to the M atom. The distances M–S have been chosen as generalized coordinate Q. These distances are proportional to the distances of the energy minimum, labeled Q_0: $Q = \alpha Q_0$. Of course, there are many vibrational modes. We have chosen a breathing mode because the force constants and the displacement of the equilibrium positions are larger than for other modes. Therefore, in principle, their effect in the lattice dynamic will be larger [47].

The changes in these ionization energies with the configuration coordinate $Q - Q_0$ are shown in Figs. 2–4 for the M_{Cu}, M_{Sn}, and M_{Zn} substitutions with M = V, Cr and Ir. The vertical line in the $Q - Q_0$ axis indicates the equilibrium position of the M–S distance in the CZTS host.

The variation with Q of the ionization energy curves (e_V, e_C, e_A and e_D) are different depending on the reference atom of the breathing mode. The Cu, Sn and Zn atoms are surrounded by 4 S atoms in the first neighboring shell at similar distances. Nevertheless, depending on the substitution, the M–S distances are different. For example, for the HLP the M–S distances are: 2.336 Å, 2.408 Å and 2.329 Å for the Cr_{Cu}, Cr_{Sn}, and Cr_{Zn} substitutions respectively. Because of the different anion–cation bond lengths (S–Cu, S–Zn, S–Sn) the anion is shifted from the middle of the anion tetrahedra and thus the tetrahedral is distorted [60].

Therefore Q_0 and $Q = \alpha Q_0$ are different for each substitution type. In addition the different shells around the M atom are also

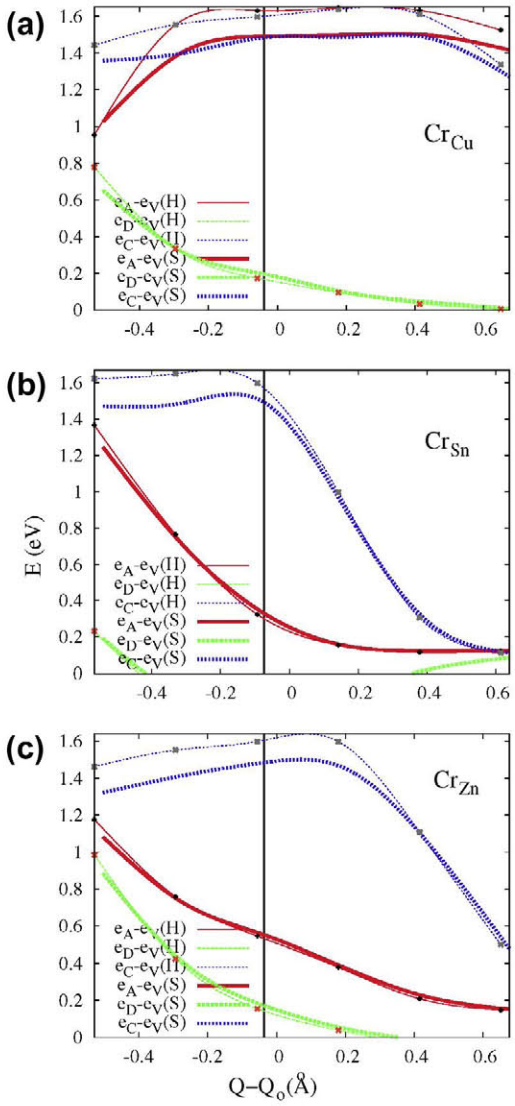

Fig. 2. Donor (e_D), acceptor (e_A) and CB edge (e_C) energies with respect to the VB edge (e_V) energy as a function of $Q - Q_0$, for the (a) M_{Cu}, (b) M_{Sn}, and (c) M_{Zn} substitution in CZTS with M = Cr. Q is the generalized coordinate (Cr–S distance) and Q_0 is its value for the energy minimum. The vertical line in the panels indicates the equilibrium position of the host CZTS semiconductor. The thick and thin lines correspond to the SLP and HLP respectively.

different. As has already been mentioned, the first shell is different for all substitutions although the first neighbors (4S) are equal because the M–S distances are different. For the remaining shells both the neighboring atoms and distances are different. For example, the neighboring second shells are 4Zn + 4Sn + 4Cu, 4Zn + 8Cu, and 4Sn + 8Cu for the Cr_{Cu}, Cr_{Sn}, and Cr_{Zn} substitutions respectively. As a consequence, the tetrahedral symmetry around the M atom is distorted. Also, the local tetrahedral symmetry around the anion S atom, with first neighbors Zn + Sn + 2Cu at different distances is distorted, From Figs. 2–4, the band gap energies obtained using the methodology described in the calculation section for the host equilibrium distance are ~1.4 eV and 1.6 eV for the HLP and SLP respectively. It compares well with the experimental results in the literature (1.4–1.6 eV [10–18]). The band gap and the ionization energies calculated from total-energy differences are in general different from the respective differences in single-particle Kohn–Sham eigenvalue energies. The latter is equivalent to using Koopman's theorem. The calculated band gap and the donor and acceptor levels calculated from total-energy differences are much

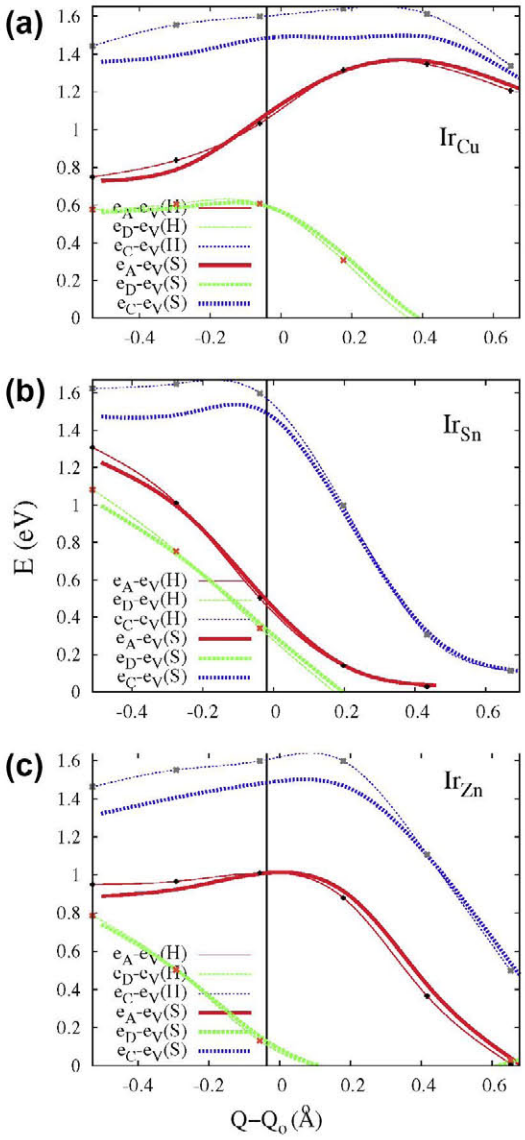

Fig. 3. Same legend as in Fig. 1, but for M = Ir.

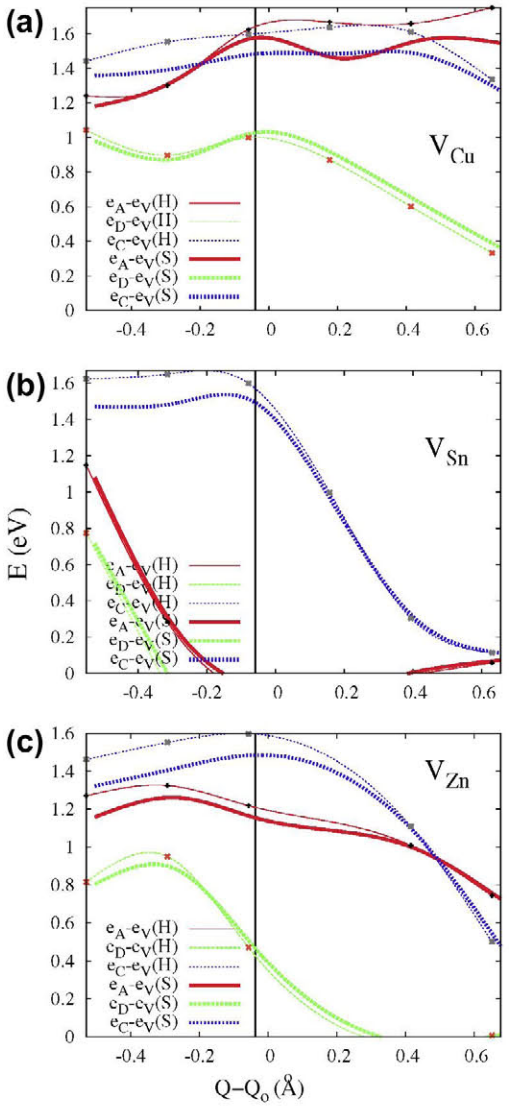

Fig. 4. Same legend as in Fig. 1, but for M = V.

closer to the experimental than those obtained from the single-particle eigenvalues, because the correlation problems and systematic errors are reduced [52].

The main difference between the ionization energies when HLP and SLP are used is the band gap. With SLP, it is lower than with HLP. This difference is larger for the inward displacements. However, the position of the acceptor and donor energies with respect to the VB edge are very similar for all Q, and for all substitutions. It can be observed that for the equilibrium position Q_0, the donor and acceptor energies for the Cr_{Zn}, Ir_{Sn}, Ir_{Cu}, and V_{Zn} substitutions are within the gap, i.e. are amphoteric.

When $Q > Q_0$ or $Q < Q_0$ the gap is reduced. The M atom, for all substitutions, is surrounded by 4S in a first shell and by 12 cation atoms in a second shell. When $Q < Q_0$ the first shell of the nearest neighbors moves closer to M, increasing the interaction and reducing the gap. For $Q > Q_0$ the outward movement causes the S anions of the first shell to come close to the cation atoms of the second shell. As a result, the anion–cation interaction increases and the gap decreases. The decrease is larger for the outward displacements because of the strong interaction of the 4S atoms with the second shell of 12 cation atoms. The bonding (anti-bonding) component of a linear combination of states decreases (increases) in energy when the interaction between these states rises. Therefore, when Q decreases and the interaction of M with the nearest neighbors increases, the ionization energies decrease (increase) if they a have bonding (anti-bonding) character.

Figs. 2–4 showing the VB and the CB edges (e_V and e_C) and the acceptor and the donor energy levels (e_A and e_D) with respect to $Q - Q_0$ can provide important information with respect to the non-radiative recombination. The simplified version of these figures based on linear energy levels with Q (total energy curves quadratic with Q) [42] is shown in Fig. 1. Comparing Fig. 1 with Figs. 2–4, the total energy curves obtained are not quadratic with Q and the ionization energy levels are not linear with Q because of the anharmonic effects not considered in the simplified model in Fig. 1.

According to the multiphonon non-radiative recombination mechanism [47,48], as the lattice vibrates in accordance with breathing mode displacements, the ionization levels move up and down in the energy gap (Figs. 1–4). For sufficiently large vibrations the level can cross into the CB or the VB and capture or emit an electron or a hole. After capture or emission the lattice near the impurity defect relaxes by means of multiphonon emission increasing the non-radiative recombination [47]. On the other hand, the lack of intersection of the level with the VB and CB greatly reduces the capture cross sections and reduces the non-radiative

recombination. From Figs. 2–4, the acceptor energy level does not cross with the CB and VB close to $|Q - Q_0| = 0$. The crossing points correspond to very high energies with respect to the equilibrium configurations. This indicates the existence of recombination barriers for the electron capture from the CB to the IB and from the IB to VB, reducing the non-radiative recombination.

The substitution energy of a host A atom by M (M_A substitution) in CZTS for growth processes that use gaseous phases rather than solids for the deposition of the modified compound, such as molecular beam epitaxy or physical vapor deposition, can be estimated as $\Delta E(A) = E(Cu_2ZnSnS_4{:}M) - E(Cu_2ZnSnS_4) + [E(A) - E(M)]$, where A = Cu, Sn or Zn, M = V, Cr and Ir, $E(Cu_2ZnSnS_4{:}M)$ and $E(Cu_2ZnSnS_4)$ are the total energies of the unit cell with and without the M impurity, and $E(A)$ and $E(M)$ are the energies of the elemental atomic reservoirs (isolated A and M atoms). $E(Cu_2ZnSnS_4{:}Cr)$ and $E(Cu_2ZnSnS_4)$ are lower by using the SLP than the HLP, indicating that these compounds with SLP are more stable energetically. However, the substitution energies are very similar with both lattice parameters. In all substituted structures the substitution energy is negative, between −100 meV and −180 meV per atom, indicating that these substitution growth processes are favorable.

The stability of these impurity atoms at cation sites is also compared as regards the respective intrinsic cation vacancies, i.e. $E[Cu_{2-x}ZnSnS_4] + xE(M) - E[(M_xCu_{2-x})ZnSnS_4]$ for Cu. These energies are negative, between −110 meV and −230 meV per atom, indicating that these substitutions are favorable as regards the intrinsic cation vacancies.

In order to estimate the potentiality of these doped-CZTS with a partially-full IB as an IB solar-cell device, we have obtained the maximum efficiency for several solar concentrations (Fig. 5), from 1 sun (1 Kw/m^2) to maximum solar concentration (~46050 suns). We have used the model described in Ref. [28], assuming that the sun is a blackbody at 6000 K, and the cell operates at 300 K, any non-radiative recombination is suppressed, carrier mobilities are infinite (no ohmic losses), and illumination comes from an isotropic gas of photons. In addition, several non-ideal recombination channels [62] can reduce the ideal maximum efficiency. The ionization energies with respect to the VB are very similar with both HLP and SLP. The main difference is the gap, larger with HLP. For the energetic position of the IB within the energy bandgap we have used the Fermi energy (between the donor and acceptor ionization energies) and 1.4 eV for the band gap energy. As previously mentioned, at low concentration the deep localized defect states act as effective non-radiative recombination centers. However, at high concentration the negative non-radiative recombination would be decreased for the partially filled IB [49,50] with amphoteric behavior. Anyway, the results in Fig. 5 are for ideal maximum efficiency.

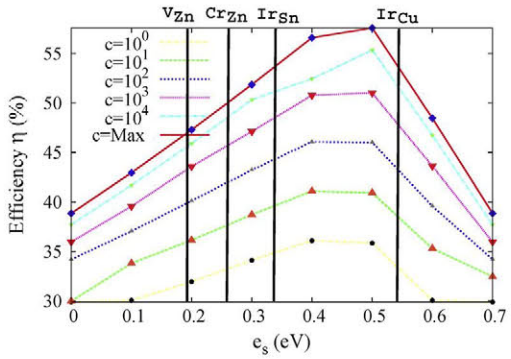

Fig. 5. Efficiency η (%) versus small gap (e_s, i.e. minimum between VB-IB and IB-CB gaps) for several sunlight concentrations (c, sun units = 1 Kw/m^2) from defect formation energy calculations. Max in the figure represents the maximum sun concentration (~46,050 suns).

The maximum efficiency of the host CZTS, from maximum solar concentration, is around a 38%. For all substitutions analyzed, the maximum efficiency of the substituted CZTS is larger than that of the host, from ~47% for V_{Zn} to ~53% for Ir_{Sn} and Ir_{Cu}. The maximums for all concentrations are also larger than the efficiency of a CZTS single-junction solar cell with equal solar concentration.

For the quaternary host systems, the VB offset between compounds with different degrees of antisite disorder is small [21,22]. Intrinsic cation disordered structures in general have a smaller bandgap than the ordered structures [23]. From some results of this work (similar ionization energies of Cr, V and Ir extrinsic substitutional impurities in two stoichiometric CZTS with a different energy band gap, i.e. with HLP and SLP), suggest that the ionization energies of Cr, V and Ir extrinsic impurities in non-stoichiometric CZTS could be similar if the substitutional extrinsic impurities do not interact with other intrinsic point defects. Because of the large variety of isolated intrinsic point defects in non-stoichiometric CZTS, additional studies are desirable in order to corroborate this fact, and to analyze the possible extrinsic impurity-intrinsic interaction of defects.

4. Conclusions

The host CZTS has been modified by introducing M impurities into substitutional cation sites in the lattice host with M = V, Cr and Ir. The ionization energies from the host and the modified CZTS have been analyzed using total energies from first-principles within density-functional theory. These ionization energies have been obtained as a function of the M–S breathing mode displacements. It can provide significant information as regards the pressure effect and non-radiative recombination, and thus, it is interesting for both spintronic and optoelectronic applications. In these analyses we have used the lattice cell parameters of both natural and synthetic CZTS. The energy band gaps obtained with these parameters compare well with the experimental results in the literature.

The donor and acceptor energies for the equilibrium position of the Cr_{Zn}, V_{Zn}, Ir_{Sn}, and Ir_{Cu} substitutions are within the gap, i.e. are amphoteric. The modification of these ionization energies with the generalized coordinate of the breathing mode indicate that the crossing points with the valence and conduction edge energies occur for larger displacements with respect to the equilibrium positions, i.e. for large energies. Thus, for this mode, the non-radiative recombination is low. An estimation of the maximum efficiency of these substituted CZTS also indicates that it can have greater efficiency than the single-gap CZTS host.

Acknowledgments

This work has been supported by the National Spanish Bibiana projects (PIB2010US-00096) and the European Commission through the funding of the project NGCPV (FP7-EU-JPN 283798), and by La Comunidad de Madrid through the funding of the project NUMANCIA-2 (Ref. N: S-2009/ENE-1477).

References

[1] N. Momose, M. Than Htay, T. Yudasaka, S. Igarashi, T. Seki, S. Iwano, Y. Hashimoto, K. Ito, Jpn J. Appl. Phys. 50 (2011) 01BG09.
[2] H. Katagiri, Thin Solid Films 480–481 (2005) 426.
[3] T. Tanaka, T. Nagatomo, D. Kawasaki, M. Nishio, Q. Guo, A. Wakahara, A. Yoshida, H. Ogawa, J. Phys. Chem. Solids 66 (2005) 1978.
[4] A. Weber, H. Krauth, S. Perlt, B. Schubert, I. Kotschau, S. Schorr, H.W. Schock, Thin Solid Films 517 (2009) 2524.
[5] N. Kamoun, H. Bouzouita, B. Rezig, Thin Solid Films 515 (2007) 5949.
[6] H. Yoo, J. Kim, Sol. Energy Mater. Sol. Cells 95 (2011) 239.

[7] K. Tanaka, M. Oonuki, N. Moritake, H. Uchiki, Sol. Energy Mater. Sol. Cells 93 (2009) 583.
[8] T. Todorov, O. Gunawan, S.J. Chey, T. Goislard de Monsabert, A. Prabhakar, D.B. Mitzi, Thin Solid Films 519 (2011) 7378.
[9] A. Ennaoui, M. Lux-Steiner, A. Weber, D. Abou-Ras, I. Kotschau, H.-W. Schock, R. Schurr, A. Holzing, S. Jost, R. Hock, T. Vo, J. Schulze, A. Kirbs, Thin Solid Films 517 (2009) 2511.
[10] G.P. Bernardini, D. Borrini, A. Caneschi, F. Di Benedetto, D. Gatteschi, S. Ristori, M. Romanelli, Phys. Chem. Miner. 27 (2000) 453.
[11] H. Matsushita, T. Maeda, A. Katsui, T. Takizawa, J. Cryst. Growth 208 (2000) 416.
[12] H. Katagiri, N. Ishigaki, T. Ishida, K. Saito, Jpn. J. Appl. Phys. 40 (2001) 500; J.-S. Seol, S.-Y. Lee, J.-C. Lee, H.-D. Nam, K.-H. Kim, Sol. Energy Mater. Sol. Cells 75 (2003) 155.
[13] F. Di Benedetto, G.P. Bernardini, D. Borrini, W. Lottermoser, G. Tippelt, G. Amthauer, Phys. Chem. Miner. 31 (2005) 683.
[14] S. Schorr, H.-J. Hoebler, M. Tovar, Eur. J. Miner. 19 (2007) 65.
[15] S. Schorr, C. Stephan, R. Mainz, H. Rodriguez-Alvarez, M. Tovar, Adv. Eng. Mater. 13 (2011) 737–741.
[16] J.J. Scragg, P.J. Dale, L.M. Peter, Electrochem. Commun. 10 (2008) 639.
[17] H. Katagiri, K. Jimbo, S. Yamada, T. Kamimura, W.S. Maw, T. Fukano, T. Ito, T. Motohiro, Appl. Phys. Express 1 (2008) 041201.
[18] K. Hönes, E. Zscherpel, J. Scragg, S. Siebentritt, Physica B 404 (2009) 4949.
[19] S. Chen, X.G. Gong, A. Walsh, S-H. Wei, Appl. Phys. Lett. 94 (2009) 041903.
[20] J. Paier, R. Asahi, A. Nagoya, G. Kressel, Phys. Rev. B 79 (2009) 115126.
[21] S. Chen, J-H Yang, X.G. Gong, A. Walsh, S-H. Wei, Phys. Rev. B 81 (2010) 245204.
[22] S. Chen, X.G. Gong, A. Walsh, S-H. Wei, Appl. Phys. Lett. 96 (2010) 021902.
[23] Y. Zhang, X. Sun, P. Zhang, X. Yuan, F. Huang, W. Zhang, J. Appl. Phys. 111 (2012) 063709.
[24] K. Biswas, S. Lany, A. Zunger, Appl. Phys. Lett. 96 (2010) 201902.
[25] C. Tablero, Thin Solid Films 520 (2012) 5011.
[26] C. Tablero, J. Phys. Chem. C 116 (2012) 23224.
[27] Z. Jun, S. LeXi, Sci China Ser E–Tech Sci 52 (2009) 269.
[28] A. Luque, A. Martí, Phys. Rev. Letts. 78 (1997) 5014; A. Luque, A. Martí, Prog. Photovoltaics 9 (2001) 73.
[29] C. Tablero, D. Fuertes Marrón, J. Phys. Chem. C 114 (2010) 2756.
[30] C. Tablero, J. Appl. Phys. 106 (2009) 073718.
[31] C. Tablero, Chem. Phys. Lett 499 (2010) 75.
[32] C. Tablero, J. Phys. Chem. A 116 (2012) 1390.
[33] C. Tablero, Phys Rev B 74 (2006) 195203.
[34] C. Tablero, Solid State Commun. 143 (2007) 399.
[35] B. Lee, L. Wang, Appl. Phys. Lett. 96 (2010) 071903.
[36] Y. Burki, P. Sshwendimann, W. Czaja, H. Berger, J. Phys.: Condens. Matter 5 (1993) 9235.
[37] Y. Burki, P. Sshwendimann, W. Czaja, H. Berger, Europhys. Lett. 13 (1990) 555.
[38] C. Tablero, Appl. Phys. Lett. 96 (2010) 121104.
[39] J.L. Merz, Phys. Rev. 176 (1968) 961.
[40] W.K. Ge, S.B. Lam, I.K. Sou, J. Wang, Y. Wang, G.H. Li, H.X. Han, Z.P. Wang, Phys. Rev. B 55 (1997) 10035.
[41] M.J. Seong, H. Alawadhi, I. Miotkowski, A.K. Ramdas, S. Miotkowska, ibid 60 (1999) R16275.
[42] Y.M. Yu, S. Nam, K.-S. Lee, Y. Dae Choi, O. Byungsung, J. Appl. Phys. 90 (2001) 807.
[43] W. Wang, A.S. Lin, J.D. Phillips, W.K. Metzger, Appl. Phys. Lett. 95 (2009) 261107.
[44] L.D. DeLoach, R.H. Page, G.D. Wilke, S.A. Payne, W.P. Krupke, IEEE J. Quantum Electron. 32 (1996) 885.
[45] R.H. Page, K.I. Schaffers, L.D. DeLoach, G.D. Wilke, F.D. Patel, J.B. Tassano, S.A. Payne, W.F. Krupke, K.T. Chen, A. Burger, IEEE J. Quantum Electron. 33 (1997) 609.
[46] I.T. Sorokina, Opt. Mater. 26 (2004) 395.
[47] D.V. Lang, C.H. Henry, Phys. Rev. Lett. 35 (1975) 1525; K.V. Boer, Survey of Semiconductor Physics, John Wiley & Sons Inc. 2002.
[48] W. Shockley, W.T. Read, Phys. Rev. 87 (1952) 62; R.N. Hall, Phys. Rev. 87 (1952) 387.
[49] A Luque, A. Martí, E. Antolín, C. Tablero, Physica B 382 (2006) 320.
[50] C. Tablero, Phys. B 404 (2009) 4023; C. Tablero, J. Appl. Phys. 108 (2010) 093114.
[51] E. Antolin, A. Marti, J. Olea, et al., Appl. Phys. Lett. 94 (2009). 042115-3.
[52] D.A. Drabold, S. Estreicher, Theory of Defects in Semiconductors, Springer, Berlin Heidelberg, 2007. pp. 28-92.
[53] J.E. Northrup, S.B. Zhang, Phys. Rev. B 47 (1993) 6791.
[54] W. Kohn, L.J. Sham, Phys. Rev. 140 (1965) A1133.
[55] J.M. Soler, E. Artacho, J.D. Gale, A. García, J. Junquera, P. Ordejon, D. Sánchez-Portal, J. Phys.: Condens. Matter. 14 (2002) 2745. and references therein.
[56] N. Troullier, J.L. Martins, Phys. Rev. B 43 (1991) 1993.
[57] L. Kleinman, D.M. Bylander, Phys. Rev. Lett. 48 (1982) 1425; D.M. Bylander, L. Kleinman, Phys. Rev. B 41 (1990) 907.
[58] O.F. Sankey, D.J. Niklewski, Phys. Rev. B 40 (1989) 3979.
[59] J. P. Perdew, K. Burke, M. Ernzerhof, Phys. Rev. Lett. 77 (1996) 3865; 78 (1997) 1396.
[60] R.S. Hall, J.T. Szymanski, J.M. Stewart, Can. Miner. 16 (1978) 131.
[61] S. Schorr, Sol. Energy Mater. Sol. Cells 95 (2011) 1482.
[62] S. Siebentritt, Thin Solid Films 535 (2013) 1–4.